Journal of Harbin Engineering University Vol 44 No. 8
ISSN: 1006-7043 August 2023

The Effects Of Radiation And Mhd Casson Nanofluid Buoyancy-Driven Mixed Convection Slip Flow On An Inclined Plate With Chemical Reactions

M. Sreedhar Babu[1], P. Naga Raju[2], E. Sivasankar[3]

[1]Department of Applied Mathematics, Yogi Vemana University, Kadapa, Andhra Pradesh, India. E-mail: msreedharyvu@gmail.com.
[2]Department of Applied Mathematics, Yogi Vemana University, Kadapa, Andhra Pradesh, India. E-mail: chinna20021996@gmail.com.
[3]Department of Applied Mathematics, Yogi Vemana University, Kadapa, Andhra Pradesh, India. E-mail: sivaesara1234@gmail.com.
* Corresponding author E-mail: chinna20021996@gmail.com, ORCID: 0009-0003-9610-2609

ABSTRACT

This inquiry examines the steady-state chemical reaction, thermal radiation, and MHD Casson nanofluid (Blood /silver (Ag)) buoyancy-driven mixed convection slips flow over a porous inclined plate. Using the similarity technique, PDEs are transformed into nonlinear ODEs. Using Maple software, the Runge-Kutta fourth-order method is used to numerically solve these equations. The impacts of different effects of the magnetic field, porosity, buoyancy force parameter, velocity, temperature, concentration slips, thermal radiation, chemical reaction parameter, thermophoresis, and Schmidt number on temperature, velocity, and concentration profiles have been examined. Nusselt number, Skin friction Sherwood no are also included. The calculated results are shown graphically and in a table. The velocity profile decreases for suction and injection over inclined plates while the Casson fluid and magnetic field parameters increase. As the values of the magnetic field, thermal radiation, and volume friction increase, the temperature increases in cases of suction and injection. As the chemical reaction parameters rise, inclined plate concentration profiles increase for suction and injection. As the Sherwood number and Nusselt number across an inclined plate increase, the impression of Eckert number, thermal radiation, and magnetic field values seems to be growing. It has many applications, such as including die-extruded polymer sheets, continuous casting, and biomedical.

KEYWORDS Joule heating, MHD, linear thermal radiation, chemical reaction, thermophoresis.

1. Introduction

The main goal of boundary layer analysis is to precisely anticipate the intricate flow properties of the boundary layer. This is a topic that many scientists who study boundary layers and heat transmission have thought about looking into. While some studies on the subject suggested using a vertical plate, others suggested using a flat plate that was either horizontal or inclined. studying boundary layers, heat, mass transmission, extruding plastic sheets, including die-extruded polymer sheets, continuous casting, spinning fibers from glass blowing, etc. Khan et al. [1] explored MHD hybrid nanofluids over a vertical plate. The effect of heat radiation and porous media on a vertical plateis shown by Badruddin et al. [2]. Khan et al. [3] explored MHD nanofluids over a curved Sheet with partial slip. The impact of dusty slip flows through an SCNT-MCNT over an endlessly inclined plate was studied by [4]. several researchers addressed the inclined and flat plates[5]–[7].

A nanofluid is a diluted suspension of sub-nanometer-sized solid particles in a base fluid like water, oil, or ethylene glycol (Cu, Al, Ag, etc.) It is possible to create new kinds of stable suspensions by using the enhanced thermal conductivity and stability provided by nanofluids. Many researchers' efforts have resulted in the development of convective transport models for nanofluids. Numerous researchers have examined a non-homogeneous model using nanofluids for studying convective transport processes and seven-slip mechanisms. Nanofluids have properties that make them potentially useful in a broad variety of heat transfer applications, including fuel cells, microelectronics, pharmaceutical procedures, car cooling, hybrid-powered engines, heat exchangers, and so on. Many researchers have been interested in nanofluid in recent years because it has higher thermal conductivity than base fluids, which are vital for heat transfer. Nanofluids, a stable suspension of a base liquid and nanoparticles, were initially described by Choi [8]. Najma Ahmed et al. [9] explored the transient MHD convective flow of fractional nanofluid across vertical plates.

The issues with magnetohydrodynamic (MHD) natural convective flow have received considerable attention from researchers in various branches of technology and science, including nuclear engineering. pumps, accelerators, generators, plasma jet engines, industrial processes in material processing, and industrial processes in metallurgy. Raghunath [10] has investigated how an MHD hybrid nanofluid flow transports heat over a stretched sheet. Sudarsana Reddy et al [11] investigate the influence of magnetic fields, and heat generation on the flow of a nanofluid across an inclined plate with a porous medium. Goyal et al.[12] examined the MHD flow of a nanofluid over an inclined plate. Mustafa [13] discussed the Buongiorno model, MHD nanofluid flow along a converging or diverging channel. several researchers addressed the MHD.[14]–[19].

Thermal radiation explains the characteristics of the electromagnetic energy produced by a material as a function of its heat, and temperature affects these characteristics. The release of heat is made possible through thermal radiation, which raises thermal diffusivity. Thermal radiation is often used in industrial and high-temperature applications, solar panels, and nuclear power plants, as well as in the production of food, energy, missiles, gas turbines, aerospace engineering, and pharmaceuticals. The influence of radiation and MHD on blood as a base fluid and gold as nanofluids over a curved surface were discussed by Khan *et al*.[20]. Shafiq et al. [21] examined the influence of thermal radiation and MHD micropolar fluid flow on the inclined sheet. Gulle et al. [22] discussed the effects of thermal radiation and MHD Jeffrey fluid flow on the inclined porous plate. Maghsoudi et al. [23] investigated the effect of non-Newtonian fluid on thermal radiation flow through an infinity of vertical flat plates.[24]–[28]

A porous substance or material is porous if it is present. Since they are formed of natural materials, biological tissues, rocks, the earth, sand, and wooden buildings all have porous media. The porosity of this material is frequently used for modifications. For example, porous media have many uses in thermal insulation, including geothermal systems, such as tissue replacement and biomedical applications, which has aroused the interest of researchers and academics to carry out more research. Barik et al. [29] studied the MHD flows of a Hybrid nanofluid over a porous Plate. Hydromagnetic free convection flows via an infinite plate in a porous media are studied by Bang Sarma et al. [30]. Many researchers are discussed by Puros Medium.[28], [31], [32].

This study of MHD Casson nanofluid buoyancy-driven mixed convection slips flows over a porous inclined plate. We employed Blood as the basis fluid and Silver (*Ag*) in this model and coupled nonlinear PDEs into ODEs by using self-similarity are used to solve the Numerical Method (RK 4th order Method) in Maple software. The impacts of so many effects of the porosity, magnetic field, buoyancy parameter, slip conditions parameters, thermal radiation, Schmidt number, and thermophoresis parameters on temperature, velocity, and concentration profiles have been examined. Nusselt number, Skin friction, and

Sherwood number are also included. The computed results are shown explicitly and in a table. It has many applications, such as including die-extruded polymer sheets, glass-blowing-spun fibers, continuous casting, and biomedical uses in antimicrobial agents, diagnostic, and drug delivery.

2. Formulation in mathematics

Consider an incompressible, steady, 2D modal, and Magnetohydrodynamic MHD Casson nanofluid flow which includes the significance over an inclined permeable plate. We employed Blood as the basis fluid and Silver (*Ag*) nanoparticle. A magnetic field of uniform intensity B_0 is provided in the y-direction, which is usual to the flow direction, with the x-axis measured along the plate. External flow has a constant velocity U_∞ and occurs in a direction parallel to the slanted plate. The plate is maintained at a constant temperature T_w whereas the ambient temperature T_∞ where $T_w > T_\infty$. The plate and ambient species concentrations as C_w and C_∞ are considered.

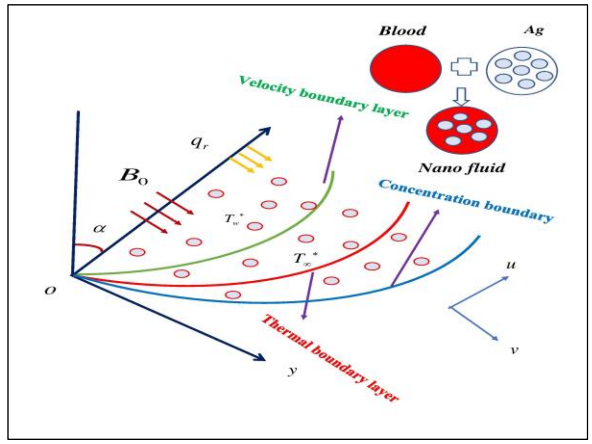

Fig 1. vertical and inclined plates Nanofluid flows diagram.

Figure 1 shows the flow diagram of the modal. The effects of MHD, radiation, Joule heating, porous media, and slips condition are all being examined. Thermophoresis is considered to get a precise look at the mass deposit on the plate's surface. The following governing equations describe continuity, momentum, or energy as flows:[33]–[35]. Casson fluid rheological model equation satisfies Das et al. [15] and Krishnart al. [36].

$$\tau = \tau_0 + \mu\beta^*$$

Equivalently

$$\tau_{ij} = \begin{cases} \left(\mu_B + \dfrac{p_y}{\sqrt{2\pi}}\right) 2e_{ij} & when\ \ \pi > \pi_c\ , \\ \left(\mu_B + \dfrac{p_y}{\sqrt{2\pi_c}}\right) 2e_{ij} & when\ \ \pi < \pi_c \end{cases} \tag{1}$$

Here τ , α^* , μ , τ_0 , and are shear stress, shear rate, dynamic viscosity, and Casson yield stress, and $\pi = e_{ij}e_{ij}$ and *eij* is the (i,j)th a factor affecting the rate of deformation, π is the non-Newtonian fluid-based product, π_c is this product's essential value, the fluid's non-Newtonian non-plastic dynamic viscosity is μ_B and p_y yield stress of the fluid. Casson fluid basic rheological equations are as follows:

$$\tau_{ij} = \mu_B \left(1 + \frac{1}{\beta}\right) 2e_{ij} \quad (2)$$

Wheres $\beta = \mu_B \frac{\sqrt{2\pi}}{p_y}$, When $\beta \to \infty$ the fluid is non-Newtonian behavior disappears and it functions much like a Newtonian fluid.

$$\frac{\partial u}{\partial x} + \frac{\partial v}{\partial y} = 0 \quad (3)$$

$$\rho_{nf}\left(u\frac{\partial u}{\partial x} + v\frac{\partial u}{\partial y}\right) = \mu_{nf}\left(1+\frac{1}{\beta}\right)\frac{\partial^2 u}{\partial y^2} + \cos\alpha\left[g\left(\rho\beta_1\right)_{nf}\left(T-T_\infty\right) + g\left(\rho\beta_2\right)_{nf}\left(T-T_\infty\right)^2\right]$$
$$+\cos\alpha\left[g\left(\rho\beta_1^*\right)_{nf}\left(C-C_\infty\right) + g\left(\rho\beta_2^*\right)_{nf}\left(C-C_\infty\right)^2\right] - \sigma_{nf}B_0^2 u - \mu_{nf}\frac{u}{k_1} \quad (4)$$

$$u\frac{\partial T}{\partial x} + v\frac{\partial T}{\partial y} = \frac{k_{nf}}{(\rho c_p)_{nf}}\left(\frac{\partial^2 T}{\partial y^2}\right) - \frac{1}{(\rho c_p)_{nf}}\frac{\partial q_r}{\partial y} + \frac{\mu_{nf}}{(\rho c_p)_{nf}}\left(\frac{\partial u}{\partial y}\right)^2 + \frac{\sigma_{nf}}{(\rho c_p)_{nf}}B_0^2 u^2 \quad (5)$$

$$u\frac{\partial C}{\partial x} + v\frac{\partial C}{\partial y} = D\left(\frac{\partial^2 C}{\partial y^2}\right) - \frac{\partial V_T C}{\partial y} - Kr\left(C-C_\infty\right)^n \quad (6)$$

Boundary conditions

$$\left.\begin{array}{ll} v = \pm v_w(x), \quad u = U_0 + L_2\frac{\partial u}{\partial y}, \quad T = T_w + L_1\frac{\partial T}{\partial y}, \quad C = C_w + L_3\frac{\partial C}{\partial y} = 0 & as \quad y \to 0 \\ u = 0, \quad T = T_\infty, \quad C = C_\infty & as \quad y \to \infty. \end{array}\right\} \quad (7)$$

Thermophysical nanofluid models are as follows:

$$\mu_{nf} = \frac{\mu_f}{(1-\phi_1)^{2.5}}, \alpha_{nf} = \frac{k_{nf}}{(\rho c_p)_{nf}}, \upsilon_{nf} = \frac{\mu_{nf}}{\rho_{nf}}.$$
$$.\rho_{nf} = (1-\phi)\rho_f + \rho_s\phi \quad (8)$$
$$(\rho C_p)_{nf} = (1-\phi)(\rho c_p)_f + \phi(\rho c_p)_s$$
$$(\rho\beta)_{nf} = (1-\phi)(\rho\beta)_f + \phi(\rho\beta)_s$$

$$\frac{\sigma_{nf}}{\sigma_f} = 1 + \frac{3\left(\frac{\sigma_s}{\sigma_f} - 1\right)\phi}{\left(\frac{\sigma_s}{\sigma_f} + 2\right) - \left(\frac{\sigma_s}{\sigma_f} - 1\right)\phi} \text{ and } k_{nf} = \left[\frac{k_s + 2k_f - 2\phi\left(k_f - k_s\right)}{k_s + 2k_f + \phi\left(k_f - k_s\right)}\right]k_f$$

Considerations include the following similarity transmutations:

$$\eta = y\sqrt{\frac{U_0}{2\nu x}},\ \theta(\eta) = \frac{T - T_\infty}{T_w - T_\infty},\ \psi = \sqrt{2\nu x U_0}\, f(\eta),\ \phi(\eta) = \frac{C - C_\infty}{C_w - C_\infty} \quad (9)$$

Steam functions are as flows

$$u = \frac{\partial \psi}{\partial y} \text{ and } v = -\frac{\partial \psi}{\partial x} \quad (10) \qquad u = U_0 f'(\eta)$$

and $v = -\sqrt{\frac{\nu U_0}{2x}}\left(f - \eta f'\right)$ (11)

Substituting Equations (9) and (11) into Equations (4) – (7) gives

$$A_1\left(1+\frac{1}{\beta}\right) f''' + A_2 f f'' + A_6 \gamma \cos\alpha\left(\theta + \delta_1\theta^2 + N(\phi + \delta_1\phi^2)\right) - A_1 K\ f' - A_3 M\ f' = 0 \quad (12)$$

$$\left(A_5 + Rd\right)\theta'' + A_4 \Pr f\theta' + A_1 \Pr Ec\left(1+\frac{1}{\beta}\right) f''^2 + A_3 \Pr EcM\left(f'\right)^2 = 0 \quad (13)$$

$$\phi'' + Scf\phi' - Sc\tau\theta'\phi' - Sc\tau\phi\theta'' - Sc\gamma_1\phi^n = 0 \quad (14)$$

Boundary condition

$$\left.\begin{array}{l} f'(0) = 1 + D_1 f''(0),\quad f(0) = S,\quad \theta(0) = 1 + D_2\,\theta'(0),\quad \phi(0) = 1 + D_2\,\phi'(0) \\ f'(\infty) = 0,\quad \theta(\infty) = 0,\quad \phi(\infty) = 0. \end{array}\right\} \quad (15)$$

In the preceding equations, we consider

$$A_1 = \frac{\mu_{nf}}{\mu_f},\ A_2 = \frac{\rho_{nf}}{\rho_f},\ A_3 = \frac{\left(\rho C_p\right)_{nf}}{\left(\rho C_p\right)_f}\ A_4 = \frac{\sigma_{nf}}{\sigma_f},\ A_5 = \frac{k_{nf}}{k_f}\ A_6 = \frac{\left(\rho\beta\right)_{nf}}{\left(\rho\beta\right)_f}$$

Here the radiation heat flux q_r , With higher orders disregarded, T^4 represents the temperature as a linear Taylor series *T* function. $T^4 \cong 4T_\infty^{\ 3}T - 3T_\infty^{\ 4}$

Analytical definitions of these parameters include the following:

$$q_r = \frac{-4\sigma^*}{3k^*}\frac{\partial T^4}{\partial y}, M = \frac{\sigma_f B_0^{\,2} 2x}{U_0 \rho_f}, Rd = \frac{4\sigma^* T_\infty^{\,3}}{3k_f k^*}, \Pr = \frac{\mu c_p}{k}, \delta_1 = \frac{g\beta_2 (T_w - T_\infty)}{\beta_1},$$
$$\delta_2 = \frac{g\beta_2^{\,*}(C_w - C_\infty)}{\beta_1^{\,*}}, \mathrm{Re}_x = \frac{U_0 2x}{\nu}, K = \frac{2x\nu}{U_0 k_1}, Ec = \frac{U_0^{\,2}}{c_p (T_w - T_\infty)}, \gamma = \frac{Gr_x}{\mathrm{Re}_x}, \tag{16}$$
$$Gr_x = \frac{g\beta_1 (T_w - T_\infty)(2x)^3}{\nu^2}, S = -v_w \sqrt{\frac{2x}{\nu U_0}}, Sc = \frac{\nu}{D}, \gamma_1 = \frac{2xKr}{U_0}(C_w - C_\infty)^{n-1}$$

It can be done to determine the thermophoretic velocity V_T via surface mass fluxing.

$$V_T = \frac{\partial T}{\partial y} = -k\nu \frac{\nabla T}{T_r} \tag{17}$$

One expression for the thermophoretic coefficient *k* is

$$k = \frac{2C_s\left(\frac{\lambda_g}{\lambda_p} + C_t K_n\right)\left[(1+K_n)\left(C_1 + C_2 e^{-C_3/K_n}\right)\right]}{\left[(1+3C_m K_n)\left(1 + 2\frac{\lambda_g}{\lambda_p} + 2C_t K_n\right)\right]} \tag{18}$$

Here C_1, C_2, C_3, C_m *and* C_s are the constants.

The thermophoretic coefficient, denoted by *k*, may take on values between $(0.2 \le k \le 1.2)$.

We may express the thermophoretic parameter as

$$\tau = -\frac{k(T_w - T_\infty)}{T_r} \tag{19}$$

3. Engineering quantities

3.1. A measure of skin friction coefficient

It is written in the following manner: $Cf_x = \frac{\tau_w}{\rho_f (U_0)^2}$. The following is a definition of shear stress:

$$\tau_w = \mu_{nf}\left(1 + \frac{1}{\beta}\right)\left(\frac{\partial u}{\partial y}\right)_{y=0} \tag{20}$$

Finally, we have

$$Cf_x \mathrm{Re}_x^{\,-1/2} = 2A_1\left(1 + \frac{1}{\beta}\right) f''(0) \tag{21}$$

3.2. Nusselt number

The heat transfer, which is denoted as the fundamental physical quantities, is

$$Nu_x = \frac{xq_w}{k_f\left(T_w - T_\infty\right)} \tag{22}$$

Where q_w is the surface heat flow in the x-direction, which is determined.

$$q_w = -\left(k_{nf} + \frac{16\sigma T_\infty^{\ 3}}{3k^*}\right)\left[\frac{\partial T}{\partial y}\right]_{y=0}$$

we have

$$Nu_x \mathrm{Re}_x^{-1/2} = -\left(A_5 + Rd\right)\theta'(0) \tag{23}$$

3.3. Sherwood number

The rate of Sherwood no, which is represented as the fundamental physical quantities, is $Sh = \frac{J_s}{U_0 C_\infty}$

(24)

Where J_s is the surface mass fluxing perceived as

$J_s = -D\left(\frac{\partial C}{\partial y}\right)_{y=0}$ than

we have

$$Sh_x \mathrm{Re}_x^{1/2} = -\phi'(0) \tag{25}$$

4. Numerical Approach

The governing equations are transformed into an initial value issue by letting

$f(\eta) = g_1,\ f'(\eta) = g_2,\ f''(\eta) = g_3,\ f'''(\eta) = g_3',\ \theta(\eta) = g_4,\ \theta'(\eta) = g_5,\ \theta''(\eta) = g_5',\ \phi(\eta) = g_6,$
$\phi'(\eta) = g_7,\ \phi''(\eta) = g_7'$. then there are reduced to

$$f''' = \frac{-\left(A_2 ff'' + A_6\gamma\cos\alpha\left(\theta + \delta_1\theta^2 + N(\phi + \delta_1\phi^2)\right) - A_1K\ f' - A_3M\ f'\right)}{A_1\left(1 + \frac{1}{\beta}\right)}$$

(26)

$$\theta'' = -\frac{\left(A_4 \Pr f\theta' + A_1 \Pr Ec\left(1 + \frac{1}{\beta}\right) f''^2 + A_3 \Pr EcM\left(f'\right)^2\right)}{\left(A_5 + Rd\right)} \tag{27}$$

$$\phi'' = -\left(Scf\phi' - Sc\tau\theta'\phi' - Sc\tau\phi\theta'' - Sc\gamma_1\phi^n \right) \tag{28}$$

Boundary conditions are

$$\left.\begin{array}{l} f(0)=S, \quad f'(0)=1+D_1 f''(0), \quad \theta(0)=1+D_2\,\theta'(0), \quad \phi(0)=1+D_2\,\phi'(0) \\ f'(\infty)=0, \quad \theta(\infty)=0, \quad \phi(\infty)=0. \end{array}\right\} \tag{29}$$

The equations (26)-(29) can be expressed as

$$\begin{bmatrix} g_1' \\ g_2' \\ g_3' \\ g_4' \\ g_5' \\ g_6' \\ g_7' \end{bmatrix} = \begin{bmatrix} g_2 \\ g_3 \\ \dfrac{-\left(A_2 g_1 g_3 + A_6\gamma\cos\alpha\left(g_4+\delta_1 g_4{}^2 + N(g_6+\delta_1 g_6{}^2)\right) - A_1 K\, g_2 - A_3 M\, g_2\right)}{A_1\left(1+\dfrac{1}{\beta}\right)} \\ g_5 \\ -\dfrac{\left(A_4 \Pr g_1 g_5 + A_1 \Pr Ec\left(1+\dfrac{1}{\beta}\right)(g_3)^2 + A_3 \Pr EcM\,(g_2)^2\right)}{\left(A_5+Rd\right)} \\ g_7 \\ -\left(Scg_1 g_7 - Sc\tau g_5 g_7 - Sc\tau g_6 g_7{}' - Sc\gamma_1 g_5{}^n\right) \end{bmatrix} \tag{30}$$

Boundary condition is

$$\left.\begin{array}{ll} g_1=S, \quad g_2=1+D_1 g_3,\ g_4=1+D_2 g_4,\ \ y_6=1+D_3 g_7, & at \ \ \eta=0 \\ y_2=0, \quad y_4=0\ \ , y_6=0 & at \ \ \eta=\infty \end{array}\right\} \tag{31}$$

Equation (30) above uses the MAPLE program and R-K4th order together with the shooting technique shown in Figure 2. As a result, the leading equations are solved in equations (31), lengthwise with their boundaries. Limiting asymptotic conditions in Equation (31) $\eta \to \infty$ was revived by an imperfect set of efforts η , says η a state when there is no discernible change in temperature, velocity, concentration profile, and all effects parameters. This performance is generally regarded as satisfactory in the domain of boundary layer investigation. When attempting to solve an issue, step scope with $\Delta\eta = 0.01$. It's better to be realistic about the inward converging condition 10^{-6} under all circumstances.

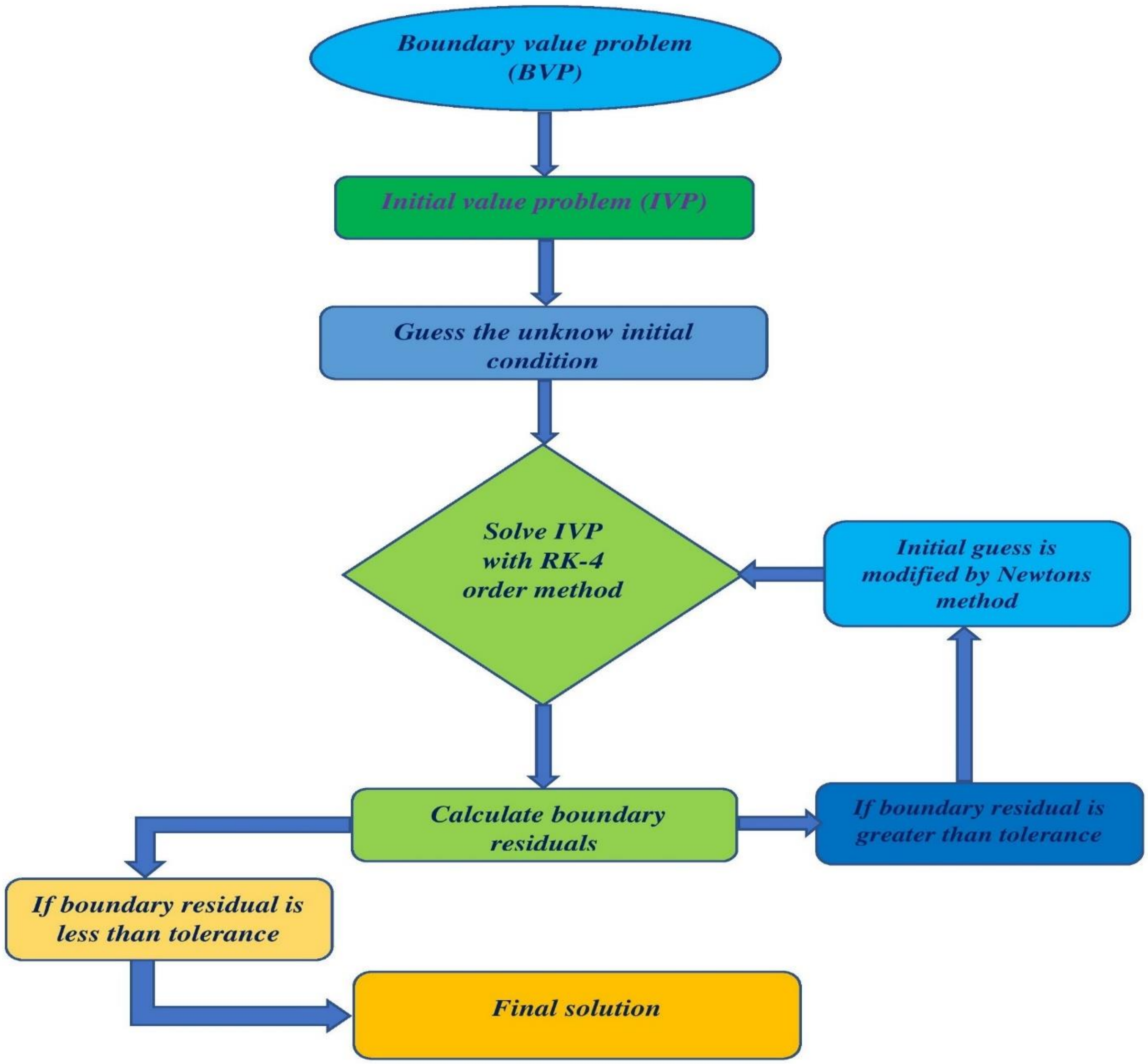

Figure 2. RK-4 Method flow chart

6. Confirmation of Results

This study of the heat transfer and mass transfer thermal radiation and mixed convection slip flow over a porous inclined plate with thermophoresis. The governing nonlinear duo Partial Differential Equations are translated into ordinary differential equations via similarity transmutations and then solved through the Maple software solver by using the Numerical Method (RK-4th Order). Dimensionless parameters values are constant in the following Rd = 0.1, $\gamma = 1$, $\phi_1 = 0.0.2$, $N = 0.5$, $\tau = 1$, K = 0.5, $D_1 = 0.3, D_2 = 0.3, D_3 = 0.3$, M = 1.0, $\delta_1 = 2, \delta_2 = 0.4$, Pr =21, Ec= 0.1, S = 0.5, $\gamma_1 = 1$, $Sc = 0.5$, $\beta = \infty$ is non-Newtonian fluid, $\beta = 2.5$ is a Newtonian fluid, $\alpha = 90^{\circ}$ is the vertical plate and $\alpha = 30^{\circ}$ is the inclined plate is considered. Table 1 displays the thermo-physical characteristics of nanoparticles. The influence of active variables, including the magnetic parameter

(M), ($S>0$) suction, ($S<0$) injection, porosity (K), α angle of inclination, buoyancy force (γ), thermal radiation (Rd), (Pr) Prandtl number, (N) is the buoyancy ratio parameter, Sc is Schmidt number, (τ) thermophoresis parameter, (Ec) Eckert number on discussed velocity profiles $f'(\eta)$, Temperature profiles $\theta(\eta)$, concentration profiles $\phi(\eta)$, skin-friction, Nusselt number, and Sherwood number for comparison of suction and injection. These parameters are represented through graphs.

6.1 Velocity profile

Figures 3-9 show the effects of the magnetic field (M), porosity (K), buoyancy force (γ), α angles vertical plate, ϕ_1 volume friction, (β) Casson fluid, (N) is the buoyancy ratio parameters, on velocity $f'(\eta)$ for inclined vertical plates. Fig. 3 demonstrates the influence of the magnetic field on the velocity $f'(\eta)$ for comparison of suction and injection over an inclined vertical plate. As the magnetic field strength rises, the $f'(\eta)$ decreases across inclined vertical plates. The magnetic force and Lorentz force they generate are together referred to as a resistive force because they decrease velocity in the physical universe. Fig. 4 protests the consequence of the Casson fluid β on the velocity $f'(\eta)$ for comparison of suction and injection over an inclined vertical plate. As the Casson fluid (β) rises, the $f'(\eta)$ decreases across inclined vertical plates. Figure 5 demonstrates the result of buoyancy force (γ) on the velocity $f'(\eta)$ over an inclined plate. As the buoyancy increases, the velocity profile rises across inclined plates for suction and injection. Fig. 6 shows the consequence of porosity (K) on the velocity $f'(\eta)$ for comparison of suction and injection over an inclined vertical plate. As the porosity (K) increases, the velocity decreases across inclined plates. As the porosity variable (K) rises, so does the friction force between nanoparticles. Figure 7 illustrates the consequence of angle (α) on the velocity $f'(\eta)$ for comparison of suction and injection over an inclined vertical plate. As the α increases, the velocity profile decreases through inclined plates. Figure 8 proves the consequence of the buoyancy ratio parameter (N) on the velocity $f'(\eta)$ over an inclined plate. As the N increases, the velocity profile $f'(\eta)$ increase for comparison of suction and injection over inclined vertical plates. Figure 9 demonstrates the result of ϕ_1 volume friction on the velocity $f'(\eta)$ over an inclined plate. As the ϕ_1 increases, the velocity profile rises across inclined plates.

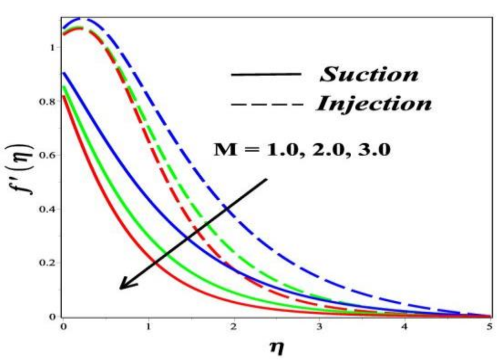

Fig. 3 The consequence of M on the $f'(\eta)$

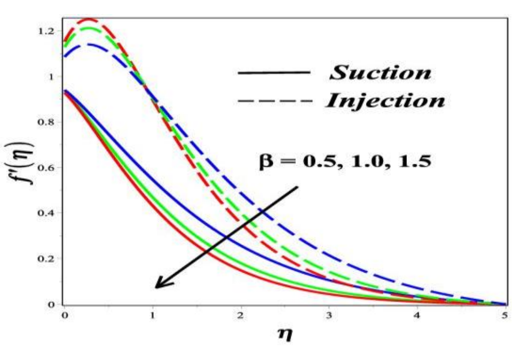

Fig. 4 The consequence of β on the $f'(\eta)$

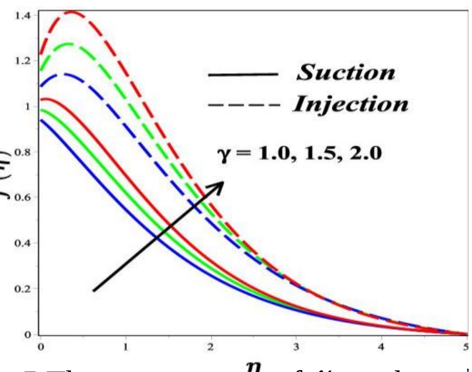

Fig. 5 The consequence of γ on the $f'(\eta)$

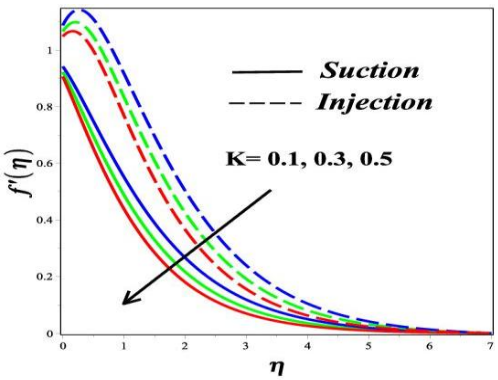

Fig. 6 The consequence of K on the $f'(\eta)$

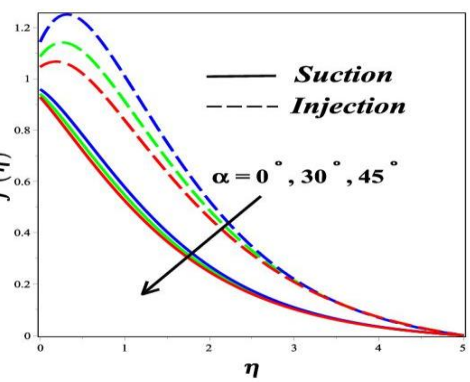

Fig. 7 The consequence of α on the $f'(\eta)$.

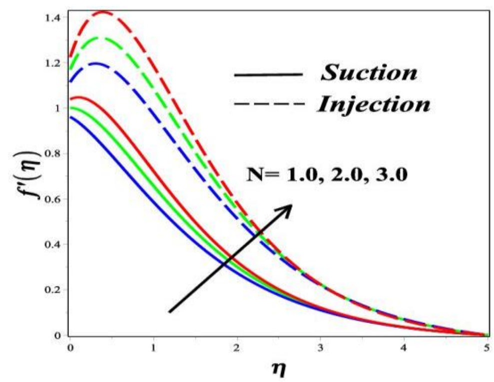

Fig. 8 The consequence of N on the $f'(\eta)$.

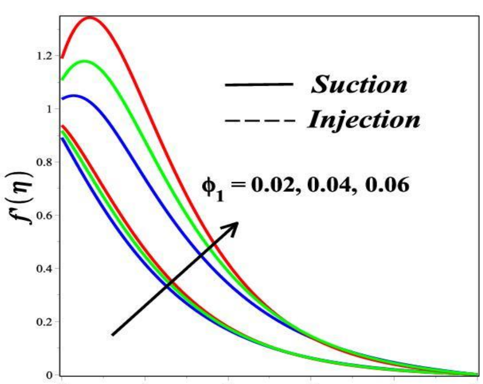

Fig. 9. The consequence of ϕ_1 on the $\theta(\eta)$.

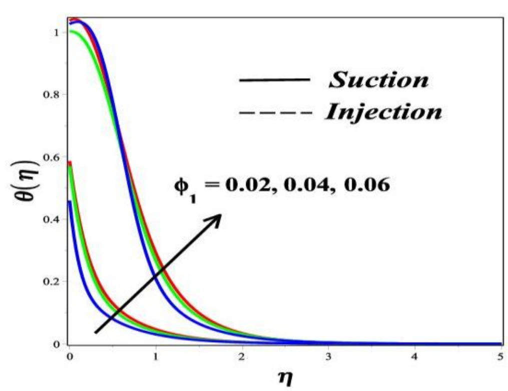

Fig. 10 The consequence of ϕ_1 on the $\theta(\eta)$.

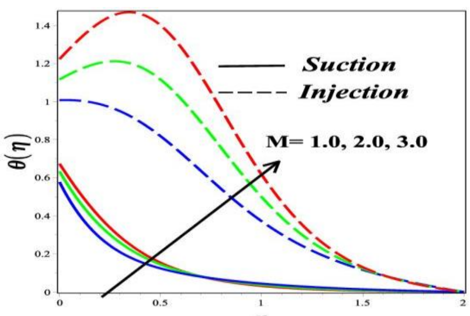

Fig. 11 The consequence of M on the $\theta(\eta)$.

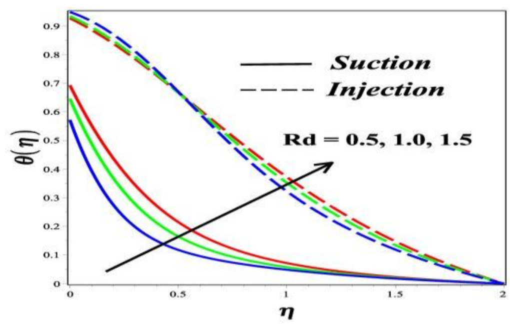

Fig. 12 The consequence of Rd on the $\theta(\eta)$.

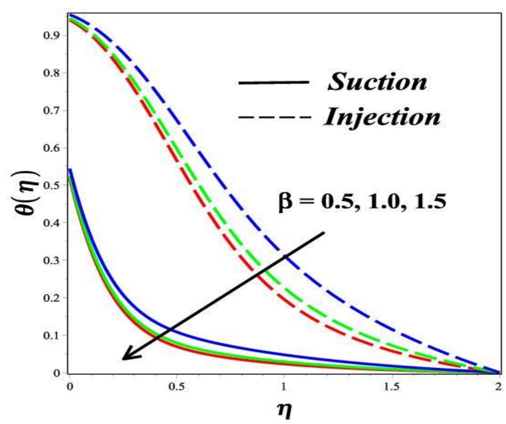

Fig. 13 The consequence of β on the $\theta(\eta)$.

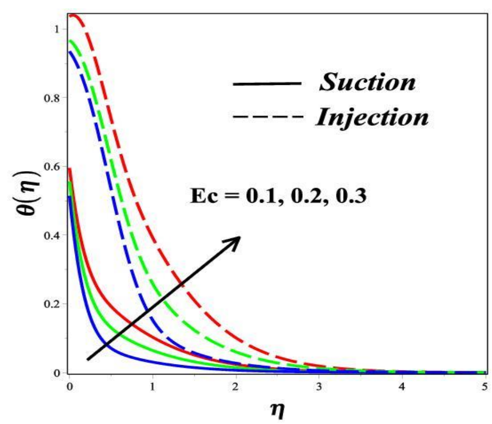

Fig. 14 The consequence of Ec on the $\theta(\eta)$
.

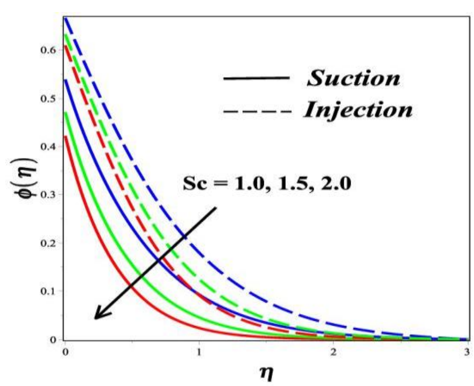

Fig. 15 The consequence of Sc on the $\phi(\eta)$

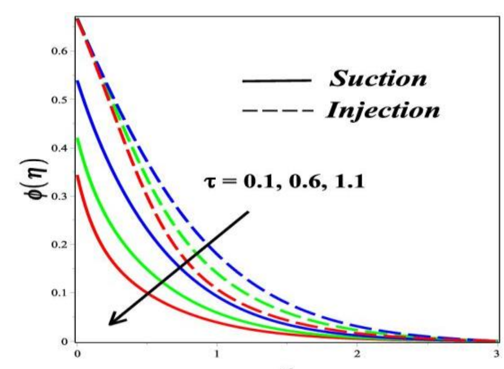

Fig. 16 The consequence of τ on the $\phi(\eta)$

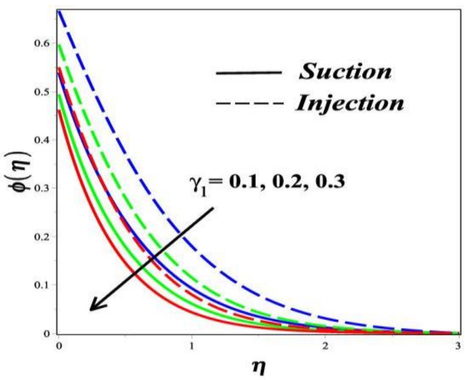

Fig. 17 The consequence of γ_1 on the $\phi(\eta)$.

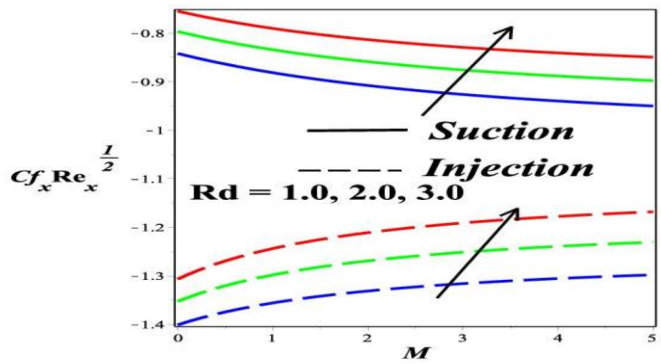

Fig. 18 The consequence of *Rd* and *M* on the $Cf_x \operatorname{Re}_x^{1/2}$

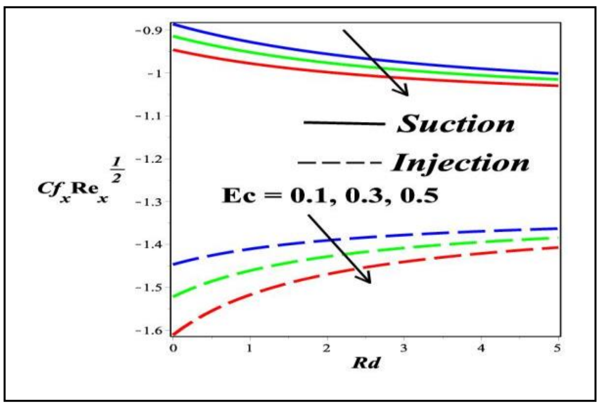

Fig. 19 The consequence of *Rd* and *Ec* on the $Cf_x \operatorname{Re}_x^{1/2}$

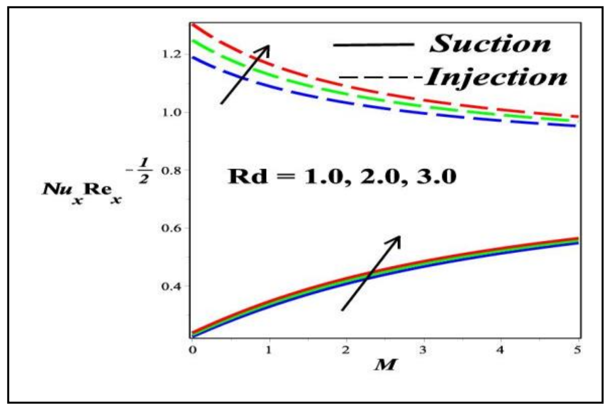

Fig. 20 The consequence of *Rd* and *M* on the $Cf_x \operatorname{Re}_x^{1/2}$

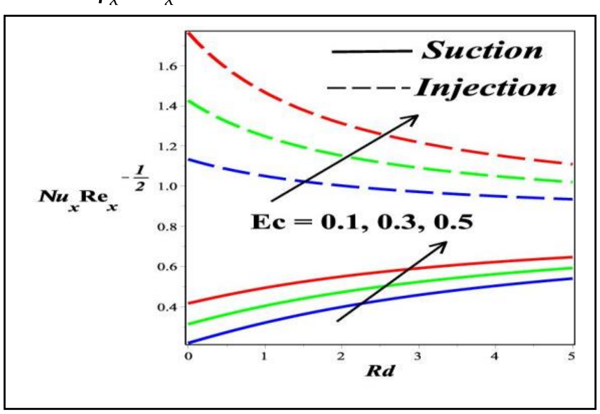

Fig. 21 The consequence of *Rd* and Ec on the $Nu_x \operatorname{Re}_x^{-1/2}$.

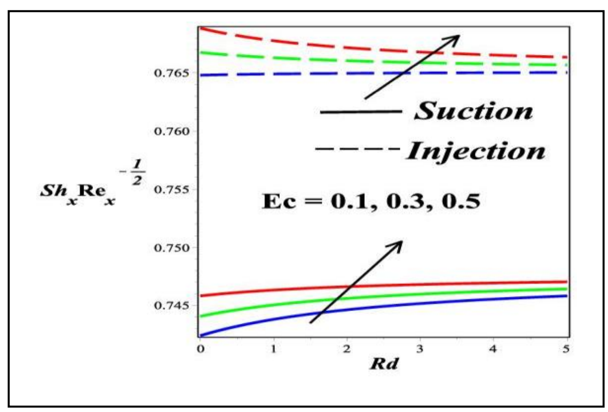

Fig. 22 The consequence of *Rd* and *Ec* on the $Sh_x \operatorname{Re}_x^{1/2}$

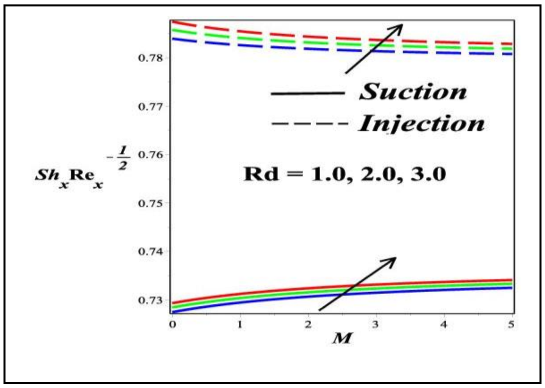

Fig. 23 The consequence of *Rd* and *M* on the $Sh_x \mathrm{Re}_x^{1/2}$

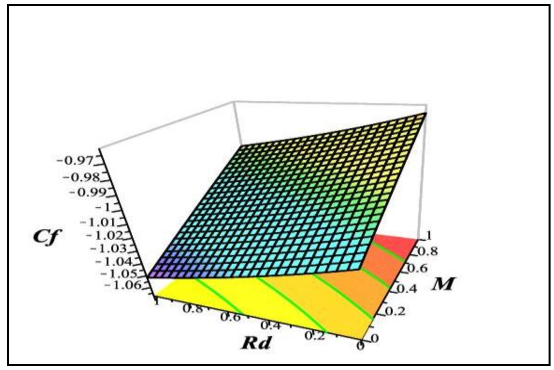

Fig. 24 The consequence of *Rd* and *M* on the $Nu_x \mathrm{Re}_x^{-1/2}$ for 3D

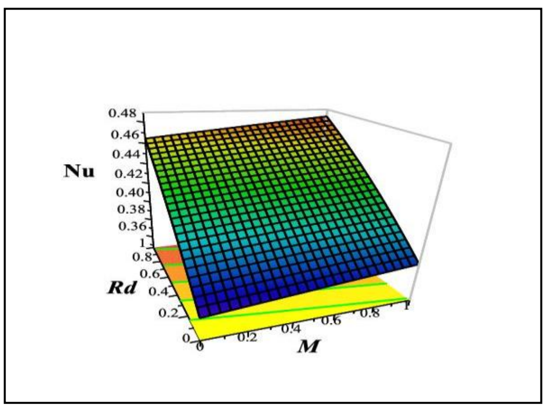

Fig. 25 The consequence of *Rd* and *M* on the $Sh_x \mathrm{Re}_x^{1/2}$ for 3D

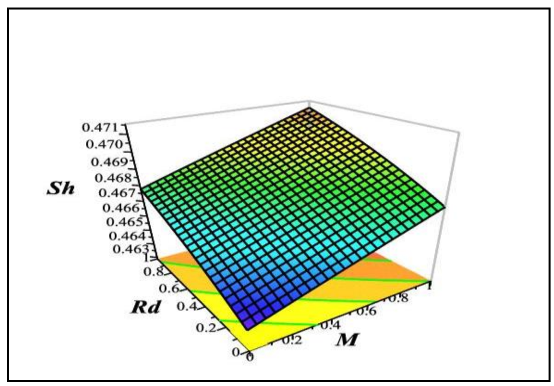

Fig. 26 The consequence of *Rd* and *M* on the $Sh_x \mathrm{Re}_x^{1/2}$ for 3D

6.2 Temperature profiles

In Figures 10-14, the inclined plates on the Temperature profile $\theta(\eta)$ are shown for several influence parameters such as *M*, *Rd*, *Ec*, ϕ_1, and β. Figures 10 show the consequences of the (ϕ_1) temperature $\theta(\eta)$ for comparison of suction and injection over inclined vertical plates. As the ϕ_1 rises, the temperature profile increases for suction and injection cases. Figures 11 demonstrate the consequences of the *M* on the temperature $\theta(\eta)$ for comparison of suction and injection over an inclined vertical plate. As the magnetic field strength grows, it also increases the temperature across the inclined plates. Physically, Due to the Lorentz force. Figure 12 shows the impression of *Rd* on temperature $\theta(\eta)$ over an inclined plate. The temperature profile rises as the Rd rises for the comparison of suction and injection over an inclined vertical plate. Physically, the fact that the thermal radiation flux rises as the flow progresses the $\theta(\eta)$ so enhances the flow development. Figure 13 shows the inspiration of the Casson fluid parameters (β) on the temperature profile $\theta(\eta)$

for comparison of suction and injection. As the Casson fluid (β)rises, the $\theta(\eta)$ decreases through inclined plates. Figure 14 shows the inspiration of the Eckert number on the temperature profile $\theta(\eta)$ for comparison of suction and injection over inclined vertical plates. As the *Ec* rises, the $\theta(\eta)$ increases through inclined plates.

6.2 Concentration profiles

Figures 15-17 show the consequence of the γ_1 chemical reactions, *Sc* which is the Schmidt number, and (τ) thermophoresis parameter on concentration profiles $\phi(\eta)$ for comparison of suction and injection cases of inclined vertical plates. Figure 17 protests the effect of *Sc* the $\phi(\eta)$ comparison of suction and injection cases on an inclined plate. As the *Sc* Schmidt number increases, the $\phi(\eta)$ profile decreases across inclined plates. Figure 16 illustrates the outcome of τ the thermophoresis parameter on concentration profiles $\phi(\eta)$ over an inclined plate. As the τ thermophoresis increases, the $\phi(\eta)$ profile decreases in both cases of suction and injection across inclined plates. Since the thermophoresis effect reduces the thermal boundary layer, this also means that the concentration boundary layer thickens as the rate of the effect rises. Figure 17 displays the consequence of γ_1 chemical reactions on the concentration profiles $\phi(\eta)$ of suction and injection across inclined plates. As the γ_1 chemical reactions increase, the $\phi(\eta)$ increase across inclined plates.

The impression of *Rd* and *M* on skin friction $Cf_x \mathrm{Re}_x^{-1/2}$ Casson nanofluid over an inclined plate is seen in Figure 18. Observing the effect of the $Cf_x \mathrm{Re}_x^{-1/2}$ many values of radiation *Rd*, *and* Magnetic field (*M)* is haggard. It has been observed that this $Cf_x \mathrm{Re}_x^{-1/2}$ is an increase in suction and injection. The effect of *Rd* and *Ec* on skin friction $Cf_x \mathrm{Re}_x^{-1/2}$ Casson nanofluid over an inclined plate is seen in Figure 19. Observing the effect of the $Cf_x \mathrm{Re}_x^{-1/2}$ many values of radiation *Rd*, *and* Ec is haggard. It has been observed that this $Cf_x \mathrm{Re}_x^{-1/2}$ is a decrease in suction and injection. The impression of *Ec*, *Rd,* and *M* on the Nusselt number $Nu_x \mathrm{Re}_x^{-1/2}$ for Casson nanofluid over an inclined plate is seen in Figures 20 and 21. Observing the effect of the $Nu_x \mathrm{Re}_x^{-1/2}$ many values of radiation *Rd*, *Ec and* Magnetic field (*M)* is haggard. It has been observed that this $Nu_x \mathrm{Re}_x^{-1/2}$ is a growing function with Rd, *Ec,* and *M* increasing for inclined plates. The impression of Ec, *Rd,* and *M* on Sherwood number $Sh_x \mathrm{Re}_x^{-1/2}$ for Casson nanofluid over an inclined plate is seen in Figures 22 and 23. Observing the effect of the $Sh_x \mathrm{Re}_x^{-1/2}$ many values of radiation *Rd*, *Ec, and* Magnetic field *M* is haggard. It has been observed that this $Sh_x \mathrm{Re}_x^{-1/2}$ for suction and injection is a growing function with Rd, *Ec,* and *M* increasing for inclined plates. The impression of *Rd* and *M* on skin friction $Cf_x \mathrm{Re}_x^{-1/2}$ $Nu_x \mathrm{Re}_x^{-1/2}$ and $Sh_x \mathrm{Re}_x^{-1/2}$ Casson nanofluid over an inclined plate for 3D diagrams is seen in Figures 24-26. As the Rd and M increase, the $Cf_x \mathrm{Re}_x^{-1/2}$, $Nu_x \mathrm{Re}_x^{-1/2}$, $Nu_x \mathrm{Re}_x^{-1/2}$ increase across inclined plates. We find excellent agreement when Table 2 compares the assessment with previously published results for the following researchers: Mills et al. [38], Tsai [39] and Alam et al. [40], and Jha and Samaila [33].

Table 1 Thermophysical properties of nanoparticles: Dolui *et al*. [37].

Property	Blood (bf)	**Silver** (Ag)
$\rho\left(kg/m^3\right)$	1063	10,500
$c_p\left(J/kgK\right)$	3594	235
$k\left(W/mk\right)$	0.492	385
$\sigma\left(s/m\right)$	0.667	6.3×10^7
$\beta\times10^{-6}\left(K^{-1}\right)$	1.8	18.7
Pr	21	-

Table.2 A comparison of Stanton numbers in some literature such consider the values $Sc=1000, M=Ec=\delta_1=\delta_2=0$ *and* $\alpha=90^\circ$.

τ	**S**	**Mills et al.** [38]	**Tsai** [39]	**Alam et al.** [40]	**Jha and Samaila** [33]	**Present results**
1	1	0.8619	0.9134	0.8691	0.8693	0.86830
1	0.5	0.5346	0.5598	0.5359	0.5368	0.53582
1	0.0	0.2095	0.2063	0.2076	0.2081	0.20714
1	-0.004	0.2068	0.2034	0.2070	0.2089	0.20853
1	-0.005	0.2062	0.2027	0.2065	0.2073	0.20716
1	-0.25	0.0344	0.0295	0.0349	0.0359	0.03529

7. Conclusions

This study employs heat transfer and mass transfer analysis of MHD Casson nanofluid buoyancy-driven mixed convection slips flow over a porous inclined plate with chemical reactions and also compares to suction and injection. The governing nonlinear coupled partial differential equations are converted into ordinary differential equations via similarity transformations. The NM is used in the MAPLE software to compute the graphical results of the flow parameters. The effects of temperature, velocity, concentration, heat transfer, skin friction coefficients, and Sherwood number on physical parameters like a magnetic field, porosity, buoyancy force and buoyancy ratio parameter, thermal radiation, chemical reactions, Schmidt number, and thermophoresis are discussed through graphs. It has many applications, such as aerodynamic extrusion of plastic sheets, including die-extruded polymer sheets, glass-blowing-spun fibers, continuous casting, and biomedical uses in antimicrobial agents, diagnostic, and drug delivery. The research's most important results are discussed here,

- ❖ The velocity profile decreases for suction and injection over inclined plates while the Casson fluid and magnetic field parameters increase.

- ❖ As the values of the thermal radiation, magnetic field, and volume friction increase, the temperature increases in cases of suction and injection.
- ❖ As the chemical reaction parameters rise, inclined plate concentration profiles increase for suction and injection.
- ❖ As the Schmidt number and thermophoresis parameters rise, inclined plate concentration profiles decrease for of suction and injection.
- ❖ As skin friction across an inclined plate is reduced, the impression of Ec, Rd, and M values rises.
- ❖ The impression of *Ec*, *Rd*, and *M* values grows as the Nusselt number and Sherwood number over an inclined plate for suction and injection rise.

NOMENCLATURE			
A	Constant	**Greek symbols**	
B_0	Magnetic field induction	T	The temperature at the surface
D_1	Velocity slip parameter	T_W	Surface Temperature
D_2	Temperature slip parameter	T_∞	Ambient Fluid temperature
D_2	Mass slip parameter	v_w	Transpiration velocity
$Cf_x \mathrm{Re}_x^{-1/2}$	Coefficient of skin friction	x, y	Axis in the direction along and normal to the plate
c_p	Specific heat	ρ	Fluid density
C_1, C_2, C_3	Constants	β	Casson fluid parameter
Ec	Eckert number	μ	Fluid dynamic viscosity
Gr_x	Local Grashof number	α_1	Temperature ratio parameter
g	Acceleration due to gravity	α_2	concentration ratio parameter
k	Thermal conductivity	β_1, β_2	Thermal expansion coefficient for temperature
K	Porosity parameter	β_1^*, β_2^*	Thermal expansion coefficient for concentration
N	Buoyancy ratio parameter	ν	Kinetic viscosity
M	Magnetic parameter	σ	Electrical conductivity
$Nu_x \mathrm{Re}_x^{-1/2}$	Nusselt number	θ	The dimensionless Temperature of a fluid
Pr	Prandtl number	ψ	Steam function
q_r	Radiative heat flux	τ_w	Wall shear stress
q_w	Surface heat flux	η	Similarity variable
Re_x	Local Reynolds number	σ^*	Stefan-Boltzmann constant
Rd	Thermal Radiation parameter	γ	Local buoyancy parameter
S	Suction / Injection parameter	λ_1	Heat generation parameter
Sc	Schmidt number	k^*	Mean absorption coefficient
β	Casson fluid parameter	γ_1	Chemical reaction parameters.

References:

[1] U. Khan, A. Zaib, S. Abu Bakar, and A. Ishak, "Stagnation-point flow of a hybrid nanoliquid over a non-isothermal stretching/shrinking sheet with characteristics of inertial and microstructure," *Case Stud. Therm. Eng.*, vol. 26, no. June, p. 101150, 2021, doi: 10.1016/j.csite.2021.101150.

[2] I. A. Badruddin, Z. A. Zainal, P. A. A. Narayana, K. N. Seetharamu, and L. W. Siew, "Free convection and radiation characteristics for a vertical plate embedded in a porous medium," *Int. J. Numer. Methods Eng.*, vol. 65, no. 13, pp. 2265–2278, 2006, doi: 10.1002/nme.1541.

[3] T. Hayat, S. Qayyum, A. Alsaedi, and B. Ahmad, "Entropy generation minimization: Darcy-Forchheimer nanofluid flow due to curved stretching sheet with partial slip," *Int. Commun. Heat Mass Transf.*, vol. 111, p. 104445, 2020, doi: 10.1016/j.icheatmasstransfer.2019.104445.

[4] M. G. Reddy, M. V. V. N. L. Sudharani, and K. G. Kumar, "An analysis of dusty slip flow through a single-/multi-wall carbon nanotube," *Contin. Mech. Thermodyn.*, vol. 32, no. 3, pp. 971–985, 2020, doi: 10.1007/s00161-019-00860-5.

[5] D. V. K. Prasad, G. S. K. Chaitanya, and R. S. Raju, "Double diffusive effects on mixed convection Casson fluid flow past a wavy inclined plate in presence of Darcian porous medium," *Results Eng.*, vol. 3, no. April, p. 100019, 2019, doi: 10.1016/j.rineng.2019.100019.

[6] S. Bilal, K. K. Asogwa, H. Alotaibi, M. Y. Malik, and I. Khan, "Analytical treatment of radiative Casson fluid over an isothermal inclined Riga surface with aspects of chemically reactive species," *Alexandria Eng. J.*, vol. 60, no. 5, pp. 4243–4253, 2021, doi: 10.1016/j.aej.2021.03.015.

[7] X. Qiang, I. Siddique, K. Sadiq, and N. A. Shah, "Double diffusive MHD convective flows of a viscous fluid under influence of the inclined magnetic field, source/sink and chemical reaction," *Alexandria Eng. J.*, vol. 59, no. 6, pp. 4171–4181, 2020, doi: 10.1016/j.aej.2020.07.023.

[8] S. K. Das, S. U. S. Choi, and H. E. Patel, "Heat Transfer in Nanofluids — A Review Heat Transfer in Nanofluids —," vol. 7632, no. 2006, 2007, doi: 10.1080/01457630600904593.

[9] N. Ahmed, N. A. Shah, B. Ahmad, S. I. A. Shah, S. Ulhaq, and M. Rahimi-Gorji, "Transient MHD convective flow of fractional nanofluid between vertical plates," *J. Appl. Comput. Mech.*, vol. 5, no. 4, pp. 592–602, 2019, doi: 10.22055/JACM.2018.26947.1364.

[10] K. Raghunath, "Study of Heat and Mass Transfer of an Unsteady Magnetohydrodynamic (MHD) Nanofluid Flow Past a Vertical Porous Plate in the Presence of Chemical Reaction, Radiation and Soret Effects," *J. Nanofluids*, vol. 12, no. 3, pp. 767–776, 2023, doi: 10.1166/jon.2023.1965.

[11] P. Sudarsana Reddy, A. J. Chamkha, and A. Al-Mudhaf, "MHD heat and mass transfer flow of a nanofluid over an inclined vertical porous plate with radiation and heat generation/absorption," *Adv. Powder Technol.*, vol. 28, no. 3, pp. 1008–1017, 2017, doi: 10.1016/j.apt.2017.01.005.

[12] M. Goyal and R. Bhargava, "Simulation of Natural Convective Boundary Layer Flow of a Nanofluid Past a Convectively Heated Inclined Plate in the Presence of Magnetic Field," *Int. J. Appl. Comput. Math.*, vol. 4, no. 2, pp. 1–24, 2018, doi: 10.1007/s40819-018-0483-0.

[13] M. Mustafa, "MHD nanofluid flow over a rotating disk with partial slip effects: Buongiorno model," *Int. J. Heat Mass Transf.*, vol. 108, pp. 1910–1916, 2017, doi: 10.1016/j.ijheatmasstransfer.2017.01.064.

[14] A. Rauf, N. Ali Shah, A. Mushtaq, and T. Botmart, "Heat transport and magnetohydrodynamic hybrid micropolar ferrofluid flow over a non-linearly stretching sheet," *AIMS Math.*, vol. 8, no. 1, pp. 164–193, 2023, doi: 10.3934/math.2023008.

[15] N. Abbas, W. Shatanawi, and T. A. M. shatnawi, "Thermodynamic study of radiative chemically reactive flow of induced MHD sutterby nanofluid over a nonlinear stretching cylinder," *Alexandria Eng. J.*, vol. 70, pp. 179–189, 2023, doi: 10.1016/j.aej.2023.02.038.

[16] K. Ahmed, T. Akbar, I. Ahmed, T. Muhammad, and M. Amjad, "Mixed convective MHD flow of Williamson fluid over a nonlinear stretching curved surface with variable thermal conductivity and activation energy," *Numer. Heat Transf. Part A Appl.*, vol. 0, no. 0, pp. 1–16, 2023, doi: 10.1080/10407782.2023.2194689.

[17] K. Sakkaravarthi and P. B. A. Reddy, "Entropy optimization of MHD hybrid nanofluid flow through a curved stretching sheet with thermal radiation and heat generation: Semi-analytical and numerical simulations," *Proc. Inst. Mech. Eng. Part E J. Process Mech. Eng.*, pp. 1–11, 2022, doi: 10.1177/09544089221100222.

[18] M. Qayyum *et al.*, "Heat Transfer Analysis of Unsteady MHD Carreau Fluid Flow over a Stretching/Shrinking Sheet," *Coatings*, vol. 12, no. 11, 2022, doi: 10.3390/coatings12111661.

[19] M. Y. Ali, S. Reza-E-Rabbi, M. M. H. Rasel, and S. F. Ahmmed, "Combined impacts of thermoelectric and radiation on hydromagnetic nanofluid flow over a nonlinear stretching sheet," *Partial Differ. Equations Appl. Math.*, vol. 7, no. February, p. 100500, 2023, doi: 10.1016/j.padiff.2023.100500.

[20] U. Khan, A. Zaib, and A. Ishak, "Magnetic Field Effect on Sisko Fluid Flow Containing Gold Nanoparticles through a Porous Curved Surface in the Presence of Radiation and Partial Slip," *Mathematics*, vol. 9, no. 9, p. 921, Apr. 2021, doi: 10.3390/MATH9090921.

[21] B. Ali, A. Shafiq, I. Siddique, Q. Al-Mdallal, and F. Jarad, "Significance of suction/injection, gravity modulation, thermal radiation, and magnetohydrodynamic on dynamics of micropolar fluid subject to an inclined sheet via finite element approach," *Case Stud. Therm. Eng.*, vol. 28, no. October, p. 101537, 2021, doi: 10.1016/j.csite.2021.101537.

[22] N. Gulle and R. Kodi, "Soret radiation and chemical reaction effect on MHD Jeffrey fluid flow past an inclined vertical plate embedded in porous medium," *Mater. Today Proc.*, vol. 50, pp. 2218–2226, 2021, doi: 10.1016/j.matpr.2021.09.480.

[23] P. Maghsoudi, G. Shahriari, H. Rasam, and S. Sadeghi, "Flow and natural convection heat transfer characteristics of non-Newtonian nanofluid flow bounded by two infinite vertical flat plates in presence of magnetic field and thermal radiation using Galerkin method," *J. Cent. South Univ.*, vol. 26, no. 5, pp. 1294–1305, 2019, doi: 10.1007/s11771-019-4088-5.

[24] Y. M. Chu *et al.*, "Thermal impact of hybrid nanofluid due to inclined oscillatory porous surface with thermo-diffusion features," *Case Stud. Therm. Eng.*, vol. 42, no. December 2022, p. 102695, 2023, doi: 10.1016/j.csite.2023.102695.

[25] B. Ahmad, M. Ozair Ahmad, M. Farman, A. Akgül, and M. B. Riaz, "A significance of multi slip condition for inclined MHD nano-fluid flow with non linear thermal radiations, Dufuor and Sorrot, and chemically reactive bio-convection effect," *South African J. Chem. Eng.*, vol. 43, no. September 2022, pp. 135–145, 2023, doi: 10.1016/j.sajce.2022.10.009.

[26] B. V. Swarnalathamma, D. M. P. Babu, and M. V. Krishna, "Combined impacts of Radiation absorption and Chemically reacting on MHD Free Convective Casson fluid flow past an infinite vertical inclined porous plate," *J. Comput. Math. Data Sci.*, vol. 5, no. November, p. 100069, 2022, doi: 10.1016/j.jcmds.2022.100069.

[27] R. N. Barik and G. C. Dash, "Thermal radiation effect on an unsteady magnetohydrodynamic flow past inclined porous heated plate in the presence of chemical reaction and viscous dissipation," *Appl. Math. Comput.*, vol. 226, pp. 423–434, 2014, doi: 10.1016/j.amc.2013.09.077.

[28] K. Sakkaravarthi and P. B. A. Reddy, "Entropy generation on Casson hybrid nanofluid over a curved stretching sheet with convective boundary condition: Semi-analytical and numerical simulations," *Proc. Inst. Mech. Eng. Part C J. Mech. Eng. Sci.*, 2022, doi: 10.1177/09544062221119055.

[29] A. Nayan, N. I. F. A. Fauzan, M. R. Ilias, S. F. Zakaria, and N. H. Z. Aznam, "Aligned Magnetohydrodynamics (MHD) Flow of Hybrid Nanofluid Over a Vertical Plate Through Porous Medium," *J. Adv. Res. Fluid Mech. Therm. Sci.*, vol. 92, no. 1, pp. 51–64, 2022, doi: 10.37934/arfmts.92.1.5164.

[30] D. Sarma and K. K. Pandit, "Effects of Hall current, rotation and Soret effects on MHD free convection heat and mass transfer flow past an accelerated vertical plate through a porous medium," *Ain Shams Eng. J.*, vol. 9, no. 4, pp. 631–646, 2018, doi: 10.1016/j.asej.2016.03.005.

[31] G. Revathi, J. B. Macherla, C. S. Raju, R. Sharma, and A. J. Chamkha, "Significance of magnetic field on Carreau dissipative flow over a curved porous surface with activation energy," *J. Nanofluids*, vol. 10, no. 1, pp. 75–82, 2021, doi: 10.1166/JON.2021.1768.

[32] S. Mukhopadhyay and G. C. Layek, "Effects of thermal radiation and variable fluid viscosity on free convective flow and heat transfer past a porous stretching surface," *Int. J. Heat Mass Transf.*, vol. 51, no. 9–10, pp. 2167–2178, May 2008, doi: 10.1016/j.ijheatmasstransfer.2007.11.038.

[33] B. K. Jha and G. Samaila, "Numerical Heat Transfer , Part B : Fundamentals Nonlinear approximation for buoyancy-driven mixed convection heat and mass transfer flow over an inclined porous plate with Joule heating , nonlinear thermal radiation , viscous dissipation , and thermophore," *Numer. Heat Transf. Part B Fundam.*, vol. 83, no. 4, pp. 139–161, 2023, doi: 10.1080/10407790.2022.2150341.

[34] A. Selim, M. A. Hossain, and D. A. S. Rees, "The effect of surface mass transfer on mixed convection flow past a heated vertical flat permeable plate with thermophoresis," *Int. J. Therm. Sci.*, vol. 42, no. 10, pp. 973–982, 2003, doi: 10.1016/S1290-0729(03)00075-9.

[35] M. S. Alam, M. M. Rahman, and M. A. Sattar, "Effects of variable suction and thermophoresis on steady MHD combined free-forced convective heat and mass transfer flow over a semi-infinite permeable inclined plate in the presence of thermal radiation," *Int. J. Therm. Sci.*, vol. 47, no. 6, pp. 758–765, 2008, doi: 10.1016/j.ijthermalsci.2007.06.006.

[36] M. V. Krishna, "Chemical reaction, heat

absorption and Newtonian heating on MHD free convective Casson hybrid nanofluids past an infinite oscillating vertical porous plate," *Int. Commun. Heat Mass Transf.*, vol. 138, no. August, p. 106327, 2022, doi: 10.1016/j.icheatmasstransfer.2022.106327.

[37] S. Dolui, B. Bhaumik, and S. De, "Combined effect of induced magnetic field and thermal radiation on ternary hybrid nanofluid flow through an inclined catheterized artery with multiple stenosis," *Chem. Phys. Lett.*, vol. 811, no. September 2022, p. 140209, 2023, doi: 10.1016/j.cplett.2022.140209.

[38] A. F. Mills, H. Xu, and F. Ayazi, "The effect of wall suction and thermophoresis on aerosol particle deposition from a laminar boundary layer on a flat plate," *Int. J. Heat Mass Transf.*, vol. 27, no. 7, pp. 1110–1113, 1984, doi: 10.1016/0017-9310(84)90127-3.

[39] R. Tsai, "A simple approach for evaluating the effect of wall suction and thermophoresis on aerosol particle deposition from a laminar flow over a flat plate," *Int. Commun. Heat Mass Transf.*, vol. 26, no. 2, pp. 249–257, 1999, doi: 10.1016/S0735-1933(99)00011-1.

[40] M. S. Alam, M. M. Rahman, and M. A. Sattar, "On the effectiveness of viscous dissipation and Joule heating on steady Magnetohydrodynamic heat and mass transfer flow over an inclined radiate isothermal permeable surface in the presence of thermophoresis," *Commun. Nonlinear Sci. Numer. Simul.*, vol. 14, no. 5, pp. 2132–2143, 2009, doi: 10.1016/j.cnsns.2008.06.008.